

## Microporous Carbon Materials from Bacterial Cellulose for Lithium–Sulfur Battery Applications

Yatong Quan<sup>1</sup>, Dongmei Han<sup>2</sup>, Yuhong Feng<sup>1,\*</sup>, Shuanjin Wang<sup>2</sup>, Min Xiao<sup>2</sup>, and Yuezhong Meng<sup>2,\*</sup>

<sup>1</sup> College of Materials and Chemical Engineering, Hainan University, 58 Ren Min Road, Hainan, Haikou 570228, China

<sup>2</sup> The Key Laboratory of Low-carbon Chemistry & Energy Conservation of Guangdong Province/State Key Laboratory of Optoelectronic Materials and Technologies, School of Materials Science and Engineering, Sun Yat-sen University, Guangzhou 510275, P. R. China

\*E-mail: [hn136.631@163.com](mailto:hn136.631@163.com), [mengyzh@mail.sysu.edu.cn](mailto:mengyzh@mail.sysu.edu.cn)

Received: 21 March 2017 / Accepted: 28 April 2017 / Published: 12 June 2017

---

The biomass-derived porous carbon materials is one of the most promising sulfur host materials for Li-S batteries applications. This work reports the preparation and application of a novel nitrogen-doped nanostructured microporous carbon materials (NMC) from sustainable bacterial cellulose (BC) subjecting to activation with KOH. The new material has a considerable specific surface area ( $1479 \text{ m}^2 \text{ g}^{-1}$ ) and high pore volume ( $1.14 \text{ g cm}^{-3}$ ), therefore it exhibits excellent electrical conductivity. The sulfur–NMC (S@NMC) composites based on NMC was synthesized via melt-diffusion method and used as the cathode material in Li-S batteries. The obtained S@NMC composite containing 68.3 wt% sulfur showed the highest rate capability and long cycling stability. The experiment results also show a high initial discharge capacity of  $1267 \text{ mAh g}^{-1}$  and capacity retention of  $995 \text{ mAh g}^{-1}$  after 500 discharge/charge cycles at a rate of 0.1C with a coulombic efficiency of 99.0 %.

---

**Keywords:** Bacterial Cellulose; Microporous carbon materials; Nitrogen-doped; Lithium-sulfur battery

### 1. INTRODUCTION

Lithium-sulfur (Li-S) battery is one of the most promising candidates as commercialized electrochemical power storage sources, such as electric vehicles, portable electronics and large-scale energy storages [1-2]. Comparing with traditional li-ion batteries, Li-S battery has a much higher theoretical specific capacity ( $1675 \text{ mAh g}^{-1}$ ) and a high energy density ( $2500 \text{ Wh kg}^{-1}$ ), due to the complicated multi-step redox reactions of the sulfur cathode rather than intercalation/deintercalation

process of conventional cathode materials in Li-ion batteries[3-4]. Additionally, choosing sulfur as the active material can benefit from the advantages of its high natural abundance, nontoxicity and low cost as well [5].

However, the commercialization of Li-S batteries has been seriously hindered by several problems including low sulfur utilization, poor long time cycling stability, rapidly capacity fading and low columbic efficiency. These issues are mainly attributed to the poor electrical conductivity of sulfur and the discharge product of lithium sulfide and the “shuttle effect” caused by polysulfides ( $\text{Li}_2\text{S}_n$ ,  $4 \leq n \leq 8$ ) dissolved in electrolyte, moreover, the large volumetric expansion (~80%) of cyclo-S8 upon lithiation is also one of important issues[6,7].

Thus, how to effectively improve the conductivity of sulfur cathode and improve the suppression of the polysulfide intermediates diffusion has become the focus of this field. Various attempts have been employed to overcome the above mentioned problems such as conductive porous frameworks like porous carbon materials [8-10], conducting polymers [11, 12], metal oxides and metal sulfides [13,14]. It has been confirmed that the introduction of conductive porous frameworks can not only trap sulfur with certain electronic conductivity and support enough space for volume expansion but also suppress the diffusion of polysulfides. What's more, based on theoretical calculation of sulfur allotropes [15], the size of  $\text{S}_8$  molecule at least in two dimensions are  $< 0.7$  nm. Thus,  $\text{S}_8$  can be accommodated into the micropores (0 to 2.0 nm) of carbon materials. Nevertheless, the fabrication procedures are always complicated and the sulfur loading in the cathode is usually not high enough [16-18].

In addition, researchers have also identified that nitrogen doping in porous carbon matrix for Li-S batteries can produce a higher conductivity and a stronger absorbability to the polysulfide species, which can enhance the cycle stability of the battery [19, 20].

Considering abovementioned, it is expected that a nitrogen-doped multi-porous carbon with both large pore volume and a small pore size is designed for the applications of Li-S batteries. Many other synthetic methods to get the porous carbons have also been reported, such as carbonization of organic or polymeric precursors [21], carbide-derived carbon (CDC) methods [22], and template synthetic methods [23].

The bio-derived carbon materials are promising due to their low cost, high availability and certain composition with doped elements and high product yield from the biosources such as straw, fruit peel, or dried small shrimps [24]. These carbons can be synthesized in a green, energy efficient and cost effective way. Bio-carbon with particular shapes and pores could be obtained via employing modern carbonization techniques. The produced carbon has high surface area and large pore volume which when used in energy storage devices, showing excellent electrochemical properties. The carbon materials from biomass, including microporous, mesoporous and hierarchically porous structure, used as sulfur host in Li-S batteries [24-27]. Moreover, the natural nitrogen doping can obviously improve the electron conductivity and strongly adsorb polysulfides, endowing a good rate capability and remarkable cycling stability for Li-S batteries.

Taking the aforementioned factors into account for this study, a nitrogen-doped nanostructured microporous carbon materials (NMC) were prepared by carbonization of form laboratory-made bacterial cellulose (BC) through a facile KOH activation method. The as-prepared NMC possess high

surface area and narrow pore size distribution, and exhibits excellent electrical conductivity which could not only improve sulfur loading, but also significantly suppress polysulfide diffusion. Moreover, the promoter of natural doped nitrogen can help improving the electron conductivity obviously and adsorption of polysulfides strongly, which contribute to good rate capability and remarkable cycling stability, demonstrating a promising matrix for stable and long-term lithium-sulfur batteries.

## 2. EXPERIMENTAL

### 2.1. Material synthesis

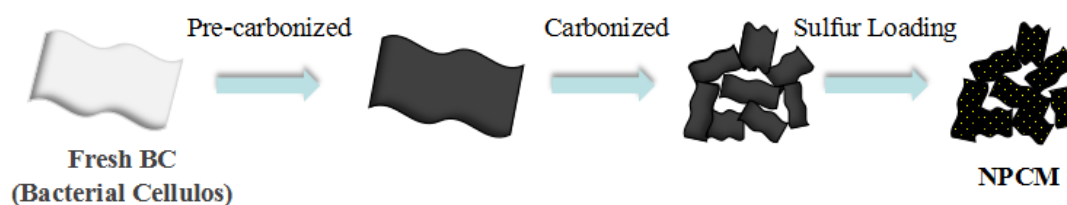


**Figure 1.** Schematic illustration for NMCs and S@NMC composites fabrication

The preparation process of NMCs and S@NMC composites are schematically illustrated in Figure 1. Bacterial cellulose hydrogels and its residual medium with enriched carbon and nitrogen were prepared and purified as previously reported [28], and then freeze-dried to get BC aerogels. They are pre-carbonized at 300°C with a heating rate of 1°C min<sup>-1</sup>. The obtained pre-carbonized BC was well-mixed with KOH at different mass ratio(w/w =1:0.5, 1:1, and 1:2), followed by stirring in a ball-milling quartz mortar for 2 h and heated in N<sub>2</sub> atmosphere at 900°C temperatures for 2 h with a heating rate of 5°C min<sup>-1</sup>. The activated carbon was washed with dilute hydrochloric acid solution and deionized water for several times. Then the obtained nitrogen-doped nanostructured microporous carbon materials (expressed as NMC) was dried at 120°C overnight. The final products were labeled with different surface areas as NMC1300, NMC1400 and NMC1500, respectively. Thereafter, the S@NMC composites were prepared via a melt-diffusion approach. In this process, sulfur powder and NMC sample were fully pulverized at different mass proportion ratio(w/w =5:5, 7:3, and 9:1) and heated at 155°C with N<sub>2</sub> protection for 24h in a sealed glass tube with a heating rate of 3 °C min<sup>-1</sup>. After cooling to room temperature, the resulting S@NMC composites were collected for further test.

### 2.2. Materials characterization.

The morphology was examined by scanning electron microscopy (SEM, JSM- JSM-6380LA, Japan Electronics). The specific surface area and pore size distribution of the samples were measured using a surface area analyzer (ASAP-2010, Micromeritics, America), and they were analyzed via Brunauer–Emmett–Teller (BET) equation and the density functional theory (DFT) method,

respectively. Electron conductivity of NMCs was tested on a semiconductor powder electron conductivity test board (Suzhou Jinge Electronic Co., Ltd., SZT-D). The X-ray diffraction (XRD) was conducted by an X'Pert Pro diffractometer using Cu K $\alpha$  radiation ( $\lambda=0.15418$  nm) with a scanning rate of 4 min<sup>-1</sup> in a 2 $\theta$  range of 10° to 80°. Raman spectra were conducted using a confocal Raman microscope (HORIBA Jobin Yvon, France) with excitation at 532 nm with a He-Ne laser. Thermogravimetric analysis (TGA) measurements for the samples were performed with a PerkinElmer Pyris Diamond TG/DTA thermal analyzer in a N<sub>2</sub> atmosphere with a heating rate of 10 °C min<sup>-1</sup>. Elemental analysis (EA) was carried out on Elementar Vario EL Cube elemental analyzer.

### 2.3. Electrochemical measurements

The electrochemical performances of the as-prepared S@NMC composite were characterized using CR2025-type coin cells with lithium metal as the anode and Celgard 2500 membrane as a separator. The cathode slurry was made by mixing the 80 wt% S@NMC composite, 10 wt% carbon black (Super P, Timcal) and 10 wt% polyvinylidene fluoride (PVDF) binder. A homogeneous slurry of the above mixture was prepared using *N*-methyl-2-pyrrolidone (NMP) as a solvent. The resulting slurry was uniformly coated onto a carbon-fiber paper (CP) and then put them into convection oven 50°C for 2 h and following vacuum oven 50°C for 24 h. The as-prepared electrodes were cut into circular disks with a diameter of 14 mm and the sulfur loading density is about 2.0 mg cm<sup>-2</sup>. The cells were assembled in an argon-filled glove box, the electrolyte contains 1 M lithium bis-trifluoromethanesulfonylimide (LiTFSI) and 2% lithium nitrate in a mixed solvent of 1,3-dioxolane(DOL) and 1,2-dimethoxyethane (DME) with volume ratio of 1:1. Cyclic voltammetry (CV) and electrochemical impedance spectroscopy (EIS) measurements were performed using the Solartron 1255 B frequency response analyzer coupled with a Solartron 1287 electrochemical interface. CV was performed at a scan rate of 0.1 mV s<sup>-1</sup> in the potential range of 1.5 to 3.0 V versus Li<sup>+</sup>/Li and EIS was performed at applied voltage of 5 mV with the frequency range from 100 kHz to 0.1 Hz respectively. Charge–discharge profiles were carried out from 1.8V to 2.6 V at different current densities under room temperature by a NEWARE battery tester.

## 3. RESULTS AND DISCUSSION

### 3.1. Characterization of NMCs and S@NMCs composites

The micro-morphology of fresh BC and NMCs were examined using SEM. As shown in Figure 2a, the fresh BC reveals a disorganized three-dimensional fibrous network-like structure. Figure 2b displays that, after pre-carbanization, the BC from fibrous structure gradually turn into three-dimensional cross-linked sheet structure. The unique porous structures are shown in Figure 2c-d., it can be seen that sulfur particles are distributed in the loose porous carbon framework structure of 70S@NMC1400 composites in Figure 2e. The special structures do not only provide an electron transfer channel, but also support sufficient space for the swell of sulfur [29-31].

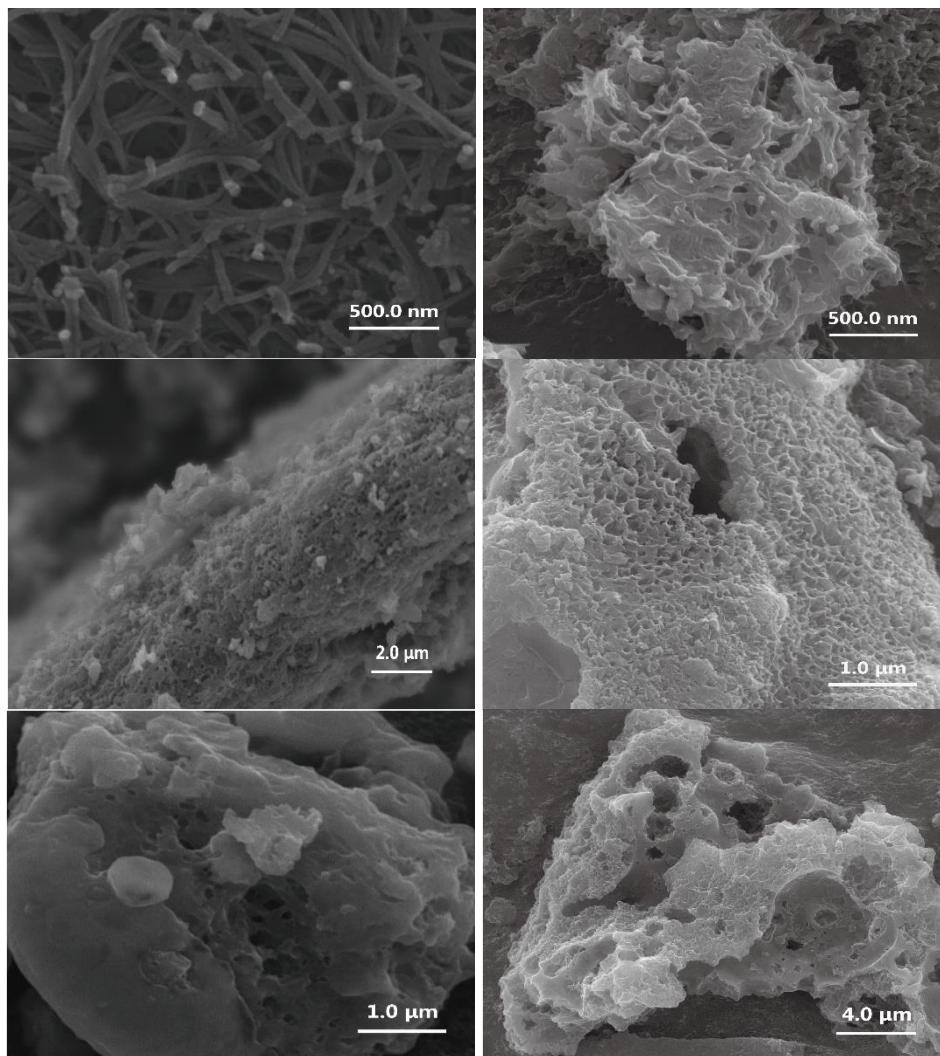


**Figure 2.** SEM images of (a) fresh Bacterial Cellulose (b) pre-carbonized BC, (c,d) NMC1400, (e) 70S@NMC1400 composite,(f) After removing S from the 70S@NMC1400 composite.

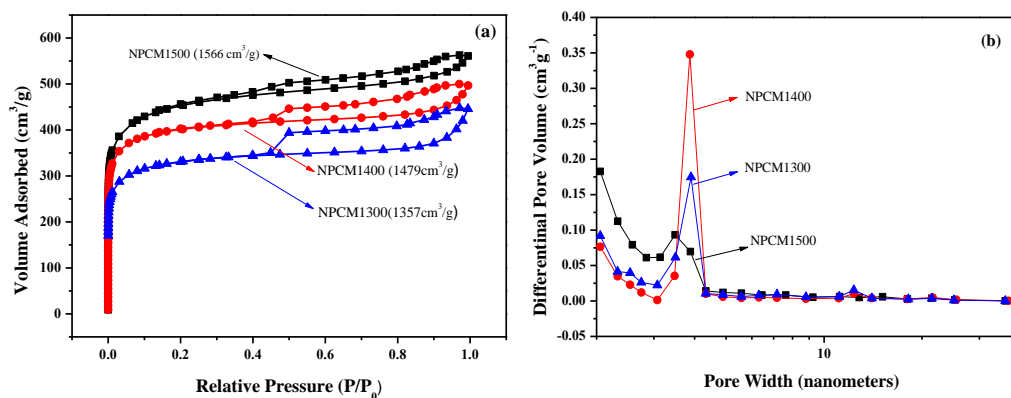


**Figure 3.** (a) Nitrogen adsorption-desorption isotherms and (b) DFT pore-size distribution curves of MCMs.

In order to observe the distribution of sulfur in the NMC1400 which was treated at 400°C for 8h to remove the physical sulfur. As shown in Figure 2f, it can be seen the uniform micropore structure, illustrating that the distribution of sulfur in 70S@NMC1400 composites.

The nitrogen adsorption-desorption isotherms were used to analyze the BET specific surface area and pore structures of the as-prepared NMCs. As shown in Figure. 3a, it clearly indicates that the BET specific surface area of NMCs decreases in the following order: NMC1500 ( $1566\text{m}^2\text{g}^{-1}$ ) > NMC1400 ( $1479\text{m}^2\text{g}^{-1}$ ) > NMC1300 ( $1357\text{m}^2\text{g}^{-1}$ ). The  $\text{N}_2$  adsorption and desorption isotherms curves of NMCs (Figure 3a) can be classified as type I according to the International Union of Pure and Applied Chemistry (IUPAC) [32]. Moreover, the distinctively elongated hysteresis loop indicates a highly accessible pore geometry with very small mesoporous, and the type I isotherms level off below the relative pressure of about 0.1(P/P<sub>0</sub>), indicating the existence of exclusive micropores in NMCs[33]. Similar results were observed for the corresponding DFT pore size distributions of NMCs. As shown in Figure 3b, the pore size ranges from approximately 0.2 to 5.0 nm, which confirms the presence of characteristic microporous structure and mesoporous structure in NMCs. Generally, the open macroporous structure favors accommodating maximum sulfur loading and facilitating electrolyte infiltration. Meanwhile, according to previous reports, the structure can accelerate the electrochemical reaction and ion diffusion process [10]. For the formation of hierarchical pores with high surface area, it may attribute to the activation of carbon with KOH, which conducts as  $6\text{KOH} + \text{C} \leftrightarrow 2\text{K} + 3\text{H}_2 + 2\text{K}_2\text{CO}_3$ [34], followed by the decomposition of  $\text{K}_2\text{CO}_3$  and/or reaction(s) of  $\text{K}/\text{K}_2\text{CO}_3/\text{CO}_2$  to yield gaseous  $\text{CO}_2$ .

It has been reported that to encapsulate sulfur with porous carbon materials is mainly expected to improve the conductivity of the sulfur cathode, therefore, the electron conductivity of the as-made carbon materials is key factor for the final electrochemical activity [35]. The electron conductivities of the as-prepared NMCs were tested at different pressure by a four-probe method and the results were listed in Table 1. It could be seen that the electron conductivity increases with increasing pressure, and the electron conductivities are ranged the same level as conductive carbon black (Super P, Timcal).

**Table 1.** Electron Conductivities of NMCs and Super P

Pressure (MPa)	Electron conductivity ( $\text{S cm}^{-1}$ )			
	NMC1500	NMC1400	NMC1300	Super P
2	4.90	5.20	6.20	7.70
4	6.80	7.60	7.70	11.0
6	8.30	10.0	8.40	14.1
8	9.50	11.6	9.70	16.3
10	13.6	16.2	14.3	20.7

The porous carbon matrix NMCs were characterized in details, X-ray diffraction (XRD) patterns were determined and two typical peaks were found at 23° and 44° (Figure 4a), which are assigned to be the (002) reflection and the superposition of (100) and (101) reflections [i.e., the (10

reflection] of the graphitic-type lattice [36]. The peak of (002) corresponds to the  $d_{(002)}$  spacing of 3.87 Å, which is significantly larger than the interlayer spacing (3.35 Å) of the typical graphite. In this case,  $\text{Li}^+$  ions is easier to insert into and extract/or run over from the porous framework of NMCs [37]. The graphitic plane (10) peak becomes gradually more apparent from NMC1300 to NMC1400 to NMC1500 with different amount of KOH, indicating the increased graphitized structures.

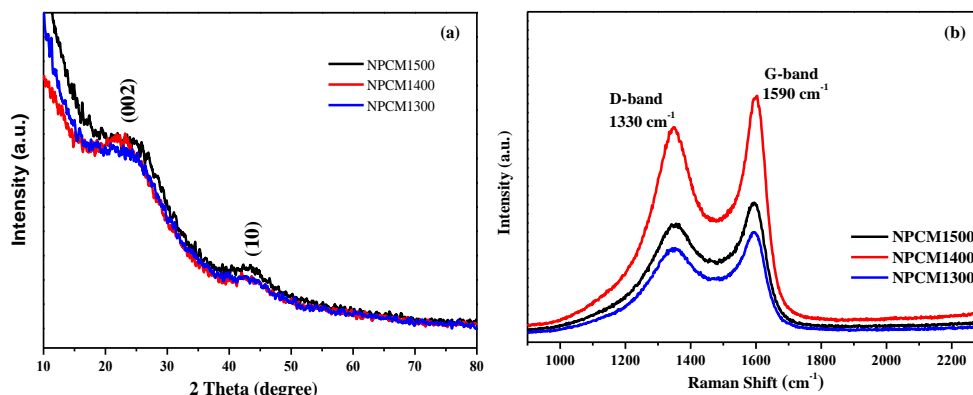


**Figure 4.** (a) XRD curves and (b) Raman curves of NMCs

The microstructure of the NMC1400 sample was further examined by Raman spectroscopy, and two obvious bands can be observed (Figure 4b), which are due to the D band and G band of carbon. The D band at around  $1330\text{ cm}^{-1}$  corresponds to a splitting of the  $E_{2g}$  stretching mode of the carbon atoms, whereas the G band at around  $1590\text{ cm}^{-1}$  should be the breathing mode of k-point phonons with  $A_{1g}$  symmetry of the carbon atoms. The integral intensity ratio ( $I_G/I_D$ ) can be used to show the defect extent and graphitization degree of the NMCs. The  $I_G/I_D$  ratios are high and change from 1.24 to 1.37, indicating that the NMCs are gradually graphitized according to XRD results. According to previous studies, the partially graphitization of NMC1400 is more helpful for electron transport [38].

**Table 2.** Specific surface area, pore volume and chemical composition of NMCs

Sample	$S_{\text{BET}}/\text{m}^2\text{g}^{-1}$	$V_{\text{total}}/\text{cm}^3\text{g}^{-1}$	$V_{\text{micro}}/\text{cm}^3\text{g}^{-1}$	Element weight ratio (%)		
				C	N	H
NMC1300	1357	1.07	0.36	85.87	1.04	1.74
NMC1400	1479	2.24	0.58	86.09	2.45	2.04
NMC1500	1566	0.77	0.46	87.76	1.63	2.25

Researchers have also identified that nitrogen doping in porous carbon matrix for Li–S batteries can produce a higher conductivity and a stronger absorbability to the polysulfide species, which will contribute to the enhanced cycle stability of the battery. [39] The element content of the three samples is also shown in Table 2. The sample NMC1400 has the highest content of nitrogen-doped of 2.45%. This is resulted from the calcination of proteins in *Acetobacter xylinum* cells and the residual culture medium. For porous carbon materials with high specific surface area and large pore volume, generally,

a narrow microporous distribution and doping nitrogen favor the improved utilization of sulfur and excellent cycle stability of Li-S battery [40]. As shown in Table 2, the sample NMC1400 is considered to be a desired carbon network for sulfur loading to fabricate S@NMC composites.

For the S@NMC1400 composites synthesized by a melt-diffusion strategy, the theoretical amount of sulfur that NMCs can accommodate is calculated according to the following process: the loading amount of sulfur equal to weight of the NMCs  $\times$  total pore volume  $\times$  density of lithium sulfide ( $1.66 \text{ g cm}^{-3}$ )  $\times$  the weight ratio of sulfur in lithium sulfide (69.78%). By this method, the theoretical capacity of sulfur in NMC1400 is 68.8 wt.%. Meanwhile, TGA measurements were used to determine the sulfur content in S@NMC1400 composites. It could be seen from Figure 5 that the NMCs exhibit a slight weight loss of approximately 8.2 wt % below 550 °C, which could be assigned to the dehydration of inside the pores and the decomposition of the functionalized groups in carbon materials [11]. For the NMC/S composites with the NMC/S ratios of (5:5, 7:3, and 9:1), the actual contents of sulfur obtained from TGA analysis are 47.4wt%, 67wt% and 82.2wt% in their turns. For S@NMC1400 composites, two weight losses can be observed. The first one below 350 °C is attributed to the evaporation of sulfur on the carbon surface, and the second loss from 350 °C to 500 °C, can be ascribed to the evaporation of sulfur in the pores of carbon matrix. However, the weight loss temperatures of 70S@NMC1400 composites are much higher than that of others and corresponding to a slowly weight loss process. It may be related to the release of sulfur confined within the micropores of NMC, which needs higher driving force and hence higher temperature to overcome the stronger capillary force [41]. This implies that sulfur is effectively restricted in the micropores of NMCs, which being consistent with theoretical calculation.

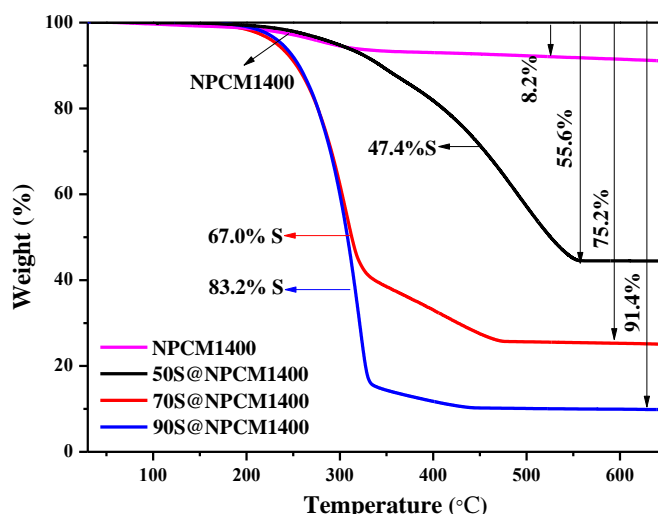


**Figure 5.** TGA curves of NMC1400 and S@NMC1400 composites

### 3.2. Electrochemical properties

The initial charge–discharge voltage curves of S@NMC composite cathode at a rate of 0.1 C are presented in Figure 6a. There are two discharge plateaus at about 2.3 V and 2.1 V, corresponding to long-chain lithium polysulfides ( $\text{Li}_2\text{S}_n$ ,  $4 \leq n \leq 8$ ) and further reduction of  $\text{Li}_2\text{S}_4$  to the final

discharged product of the short-chain  $\text{Li}_2\text{S}_2/\text{Li}_2\text{S}$  respectively. The charge plateau at about 2.4 V represents the reverse reaction from sulfides to polysulfides and finally to sulfur. [20-22,25]. As shown in figure 6a, the 50S@NMC1400 composite cathode exhibits the highest initial discharge specific capacity of  $1207 \text{ mAh g}^{-1}$ , the 70S@NMC1400 and 90S@NMC1400 composite cathodes deliver high initial discharge capacities of 1129 and  $1020 \text{ mAh g}^{-1}$ , in their turns.

To demonstrate the superiority of the 50S@NMC1400, 70S@NMC1400 and 90S@NMC1400 cathodes, the rate performance of the electrode were investigated at different current densities from 0.1 to 2 C and then reverse to 0.1 C, as shown in Figure 6b. The 70S@NMC1400 composite cathode delivers specific capacities of about 1107, 889, 784, 716 and  $592 \text{ mAh g}^{-1}$  at rates of 0.1, 0.2, 0.5, 1, and 2C, in their turns. The high discharge capacity of  $582 \text{ mAh g}^{-1}$ , achieved at the highest current rate of 2C, indicates the outstanding rate capability of 70S@NMC1400. Moreover, as the current density is decreased from 2 to 0.1 C rate after 55 cycles, a discharge capacity up to  $953 \text{ mAh g}^{-1}$  can be recovered. The excellent rate performance of 70S@NMC1400 composite cathode is attributed to the high electron conductivity and micropore structure and of the carbon host [42].

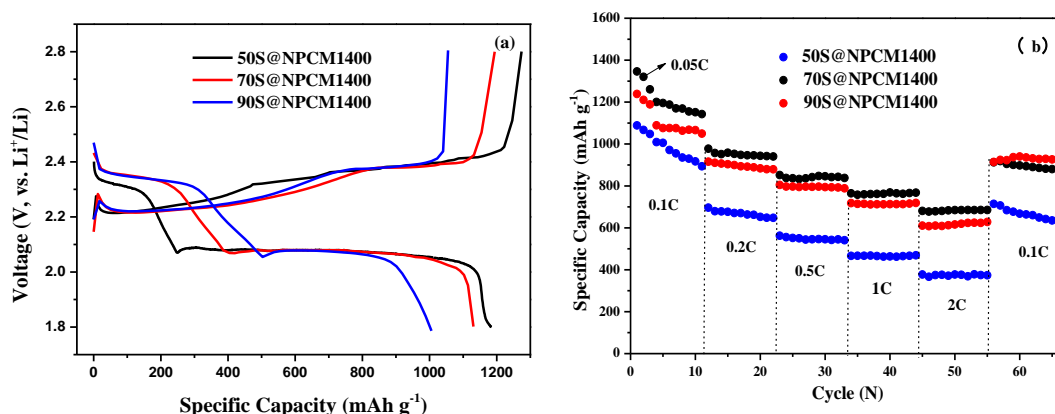


**Figure 6.** Electrochemical performances of S@NMC composite cathode. (a) Initial three charge–discharge profiles at a rate of 0.1 C, (b) rate capability at various C rates.

The long-term cycling stability of the 70S@NMC1400 composites cathodes at a rate of 0.1C were taken in the voltage window of 2.8-1.6 V at room temperature are shown in Figure 7. The capacity of 70S@NMC1400 cathode with 67.0 wt % sulfur content presents a very high initial specific capacity of  $1129 \text{ mAh g}^{-1}$ . After 500 cycles, the specific capacity of the 70S@NMC1400 composites cathodes was still kept at  $964 \text{ mAh g}^{-1}$ , the capacity retention is 85.4% and capacity attenuation per cycle is 0.03%. This results demonstrates the best cycling stability and the highest capacities among S@NMC1400 composites. Moreover, it shows high coulombic efficiency over 98% over the 500 cycles. However, the specific capacities of 50S@NMC1400 and 90S@NMC1400 decrease faster than that of 70S@NMC1400 during cycling test. The high initial specific capacities of these S@NMC1400 composites are due to the excellent electron conductivity and very suitable porous structure of NMC1400 carbon host matrixes, which can effectively promote the electrochemical reaction of sulfur. In the charge-discharge process, their micropores structure not only could trap sulfur, but also provide

spaces for volume expansion of sulfur, and it could be seen the similar method in the references [43,44]. As a result, the prepared NMC from BC are promising matrixes for suppressing the shuttling phenomenon and enhancing the utilization rate of sulfur in Li-S batteries.

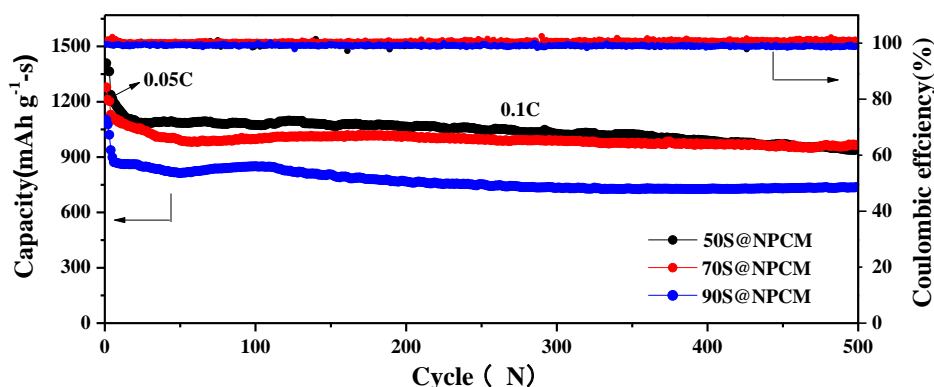


**Figure 7.** Cycling performance of 50S@NMC1400, 70S@NMC1400 and 90S@NMC1400

**Table 3.** Microporous, mesoporous and hierarchical porous carbons derived from biomass used as electrode materials and their properties for Li-S batteries

Biomass source	Obtained structure	Surface area (m <sup>2</sup> g <sup>-1</sup> )	Pore volume (cm <sup>3</sup> g <sup>-1</sup> )	S (wt.%)	Initial capacity (mAh g <sup>-1</sup> )	Retention rate	Ref.
Bacterial cellulose	N-doped microporous carbon	1479	2.24	67	1129 at 0.1C	85.4% (500 cycles at 0.1C)	This work
Camboo biochar	Microporous biochar	791.8	0.38	50	1295 at 0.1C	58.4% (50 cycles at 0.1C)	[45]
Coconut shells	Ultra microporous	1600	0.66	45.8	1458 at 0.2C	28.2% (400 cycles at 0.2C)	[46]
Hair	N-doped microporous carbon	/	/	65	1113 at 0.2C	88.3% (300 cycles at 0.2 C)	[47]
Glucose	Hierarchical porous carbon spheres	699.76	0.47	60	1253.5 at 0.1C	67.8% (50 cycles at 0.1 C)	[48]
Cotton	Hierarchical micro-macropores	1286	1.15	67	1017 at 0.2C	74.7% (200 cycles at 0.2 C)	[49]
Corn cob	Nanosheet microporous	1198	0.672	44	1600 at 0.1C	34.6% (50 cycles at 0.1 C)	[50]

Some performances of the microporous mesoporous and hierarchical porous carbons derived from biomass and the resulting properties obtained for Li-S batteries are summarized in Table 3. This work shows very high sulfur content for cathodes made from different biomass based carbon composites. And the S@NMC based cathode also shows the higher initial capacity at 0.1 C and the very high retention rate after 500 cycles at 0.1 C. The S@NMC cathode exhibit excellent electrochemical behavior because of the Large specific surface area and narrow pore distribution [25]. Thus, the high re-order polysulfides desire could not form during the reaction and the shuttle effect can

be avoided. As a result, excellent cycling stability, electrolyte compatibility and high rate capability are obtained.

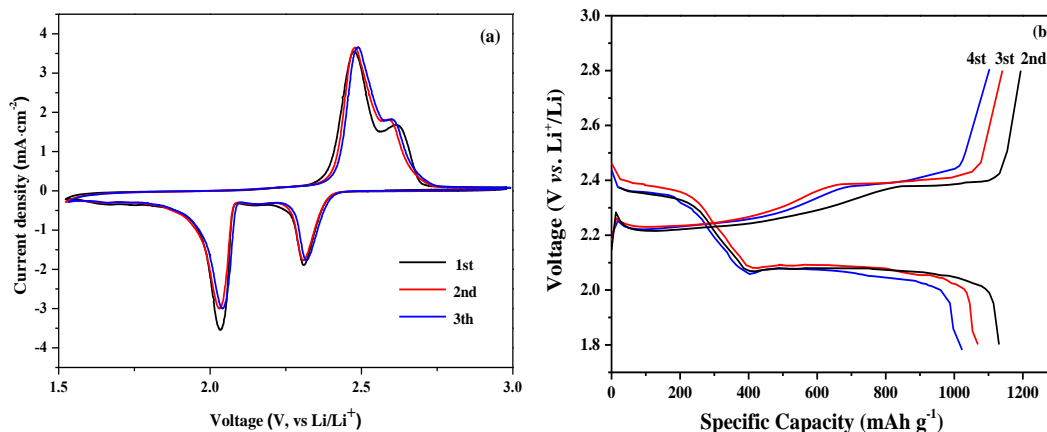


**Figure 8.** (a) CV curves for the initial three cycles of 70S@NMC1400 composite, (b) Initial charge-discharge curves of 70S@NMC1400 composite at a rate of 0.1C

In order to examine the electrochemical properties of the 70S@NMC1400 composites, cyclic voltammograms (CVs) curves of 70S@NMC1400 composite cathode in the voltage range of 1.5–3.0 V were recorded at a sweep scan rate of  $0.02 \text{ mV s}^{-1}$ , as shown in Figure 8a. At the first cathodic scan, the first reductive peak at 2.32 V is due to the reduction of elemental sulfur to soluble polysulfides ( $\text{Li}_2\text{S}_n$ ,  $2 \leq n \leq 8$ ). The second reductive peak at 2.03 V, which can be ascribed to the transformation of soluble polysulfides to  $\text{Li}_2\text{S}_2/\text{Li}_2\text{S}$ . In the first anodic scan, there is one oxide peak at about 2.37 V, which corresponds to the oxidation of  $\text{Li}_2\text{S}_2$  and  $\text{Li}_2\text{S}$  to the polysulfides [51]. We can observe that a small shoulder around at 2.40 V and can be considered to the further oxidation of polysulfides to elemental sulfur  $\text{S}_8$  [29]. For the following scans, the cathodic and anodic peaks maintain almost overlap, revealing the steady electrochemical reduction and oxidation reactions. Moreover, as shown in Figure 8b, the galvanostatic charge-discharge curves of 70S@NMC1400 composite cathode at 0.1C. It shows that two discharge plateaus at about 2.3 V and 2.1 V and only one charge plateau at 2.1 V, which is consistent with the results of CV measurements [52].

The fast reaction kinetics of 70S@NMC1400 cathode before and after cycles was further proved by the electrochemical impedance spectra (EIS) as shown in Figure 9. Both of the measured impedance curves are composed of a high-to-medium frequency region and a straight-sloped line, which are related to the charge-transfer resistance ( $R_{ct}$ ) and the mass-transfer process respectively [28–30]. After 30 cycles, the charge transfer resistance apparently decreases, indicating a fast charge transfer and excellent electrolyte infiltration attributing to the improved electrical conductivity by nitrogen doping and good electrical contact of sulfur particles with NMC1400.

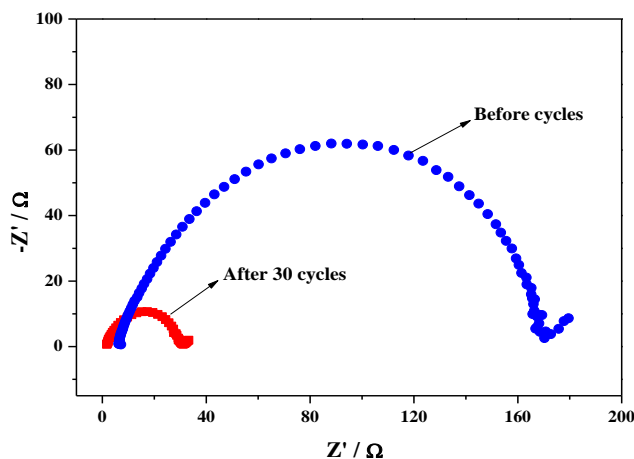


**Figure 9.** Electrochemical impedance spectra before of 70S@NMC1400 composite

#### 4. CONCLUSIONS

In summary, the nitrogen-doped multiporous carbon (NMCs) with widespread biological cell (bacterial cellulose) were successfully synthesized with a KOH activation method. NMC1400 possess a high specific surface area ( $1479 \text{ m}^2 \text{ g}^{-1}$ ) with pore volume ( $2.24 \text{ g cm}^{-3}$ ), and has the same level electron conductivities as conductive carbon black. Meanwhile, the doping nitrogen (2.45%) in the carbon network can improve the electron conductivity and provide a strong absorption ability of polysulfides, which is very suitable for the host matrix to encapsulate sulfur cathodes.

The experiment results demonstrated that S@NMC1400 cathode exhibits an excellent electrochemical performance with high initial discharge capacity, low capacity decay rate and good rate capability. It gives a high initial specific capacity of  $1129 \text{ mAh g}^{-1}$  at 0.1C and kept at  $964 \text{ mAh g}^{-1}$  after 500 cycles, together with a 0.03% capacity attenuation per cycle. These superior electrochemical performances may mainly attribute to the excellent electron conductivity and the unique microporous structure of the BC derived carbon host matrix, which are key infactor for improving the utilization of sulfur and trapping the dissolution of polysulfides.

#### ACKNOWLEDGEMENTS

The authors would like to thank the Link Project of the National Natural Science Foundation of China and Guangdong Province (Grant No. U1301244); National Natural Science Foundation of China (Grant Nos. 51573215, 21506260); Guangdong Province Science & Technology Foundation (2011B050300008); Guangdong Natural Science Foundation (Grant Nos. 2014A030313159, 2016A030313354); Guangdong Province Sci & Tech Bureau (Key Strategic Project Grant No. 2016B010114004); Guangzhou Scientific and Technological Planning Project (2014J4500002, 201607010042) for financial support of this work.

#### References

1. J. R. Akridge, Y. V. Mikhaylik and N. White, *Solid State Ionics*, 175 (2004) 243-245.
2. B. Scrosati and J. Garche, *J. Power Sources*, 195 (2010)2, 2419-2430.

3. P. G. Bruce, S. A. Freunberger, L. J. Hardwick and J. M. Tarascon, *Nat. Mater.*, 11 (2012), 19-29.
4. A. Manthiram, S. H. Chung and C. Zu, *Adv. Mater.* 27(2015) 1980-2006.
5. R. Elazari, G. Salitra, A. Garsuch, A. Panchenko and D. Aurbach, *Adv. Mater.*, 23(2011) 5641-5644.
6. J. Jiang, J. Zhu, W. Ai, X. Wang, Y. Wang, C. Zou, W. Huang and T. Yu, *Nat. Commun.*, 6(2015) 8622-8630.
7. N. Jayaprakash, J. Shen, S. S. Moganty, A. Corona and L. A. Archer, *Angew. Chem.*, 50 (2011) 5904-5908.
8. S. H. Chung and A. Manthiram, *Adv. Mater.*, 26(2014) 1360-1365.
9. C. Wang, J.J. Chen, Y.N. Shi, M.S. Zheng and Q.F. Dong, *Electrochim. Acta.*, 55 (2010) 7010-7015.
10. H. Ye, Y.X. Yin, S. Xin and Y. G. Guo, *J. Mater. Chem. A*, 22 (2013) 6602-6608.
11. J. Wang, J. Chen, K. Konstantinov, L. Zhao, S.H. Ng, G.X. Wang, Z.P. Guo and H.K. Liu, *Electrochim. Acta.*, 51 (2006) 4634-4638.
12. W. Zhou, Y. Yu, H. Chen, F.J. DiSalvo and H.D. Abruna, *J. Am. Chem. Soc.*, 135 (2013) 16736-16743.
13. B. Ding, L. Shen, G. Xu, P. Nie and X. Zhang, *Electrochim. Acta.*, 107 (2013) 78-84.
14. Z. Wei She, W. Li, J.J. Cha, G. Zheng, Y. Yang, M.T. McDowell, P.C. Hsu and Y. Cui, *Nat. Commun.* 4 (2013) 1331.
15. S. Xin, L. Gu, N. Zhao, Y. Yin, L. Zhou, Y. Guo, and L. Wan, *J. Am. Chem. Soc.*, 134 (2012) 45, 18510-18513.
16. H. Li, L. Sun, and G. Wang, *ACS Appl. Mater. Inter.*, 8 (2016) 6061-6071.
17. J. Wang, Y. Yang and F. Kang, *Electrochim. Acta.*, 168(2015) 271-276.
18. G. Ma, Z. Wen, Q. Wang, C. Shen, P. Peng, J. Jin and X. Wu, *J. Power Sources*, 273 (2015) 511-516.
19. J. Liang, Z. Sun, F. Li and H. Cheng, *Energy Storage Mater.*, 2 (2015) 76-106.
20. Z. Li, Y. Huang, L. Yuan, Z. Hao, and Yunhui Huang, *Carbon*, 92 (2015) 41-63.
21. H. L. Jiang, B. Liu, Y. Q. Lan, K. Kuratani, T. Akita, H. Shioyama, F. Zong and Q. Xu, *J. Am. Chem. Soc.*, 133 (2011) 11854-11857.
22. A. Shaikjee and N. J. Coville, *Carbon*, 50 (2012) 3376-3398.
23. V. Presser, L. Zhang, J. J. Niu, J. McDonough, C. Perez, H. Fong and Y. Gogotsi, *Adv. Energy Mater.*, 1 (2011) 423-430.
24. B. Zhang, M. Xiao, S. J. Wang, D. M. Han, S. Q. Song, G. H. Chen and Y. Z. Meng, *ACS Appl. Mater. Inter.*, 6 (2014) 13174-13182.
25. Z. J. Sun, M. Xiao, S. J. Wang, D. M. Han, S. Q. Song, G. H. Chen and Y. Z. Meng, *J. Mater. Chem. A*, 2 (2014) 9280-9286.
26. H. L. Jiang, B. Liu, Y. Q. Lan, K. Kuratani, T. Akita, H. Shioyama, F. Zong and Q. Xu, *J. Am. Chem. Soc.*, 133 (2011) 11854-11857.
27. A. Shaikjee and N. J. Coville, *Carbon*, 50 (2012) 3376-3398.
28. J. Yang, D. Sun, J. Li, X. Yang, J. Yu, Q. Hao, W. Liu, J. Liu, Z. Zou and J. Gu, *Electrochimica Acta.*, 54 (2009) 6300-6305.
29. V. Presser, L. Zhang, J. J. Niu, J. McDonough, C. Perez, H. Fong and Y. Gogotsi, *Adv. Energy Mater.*, 1 (2011) 423-430.
30. S. H. Chung, C. H. Chang, and A. Manthiram, *ACS nano*, 11 (2016) 10462-10470.
31. M. Kruk and M. Jaroniec, *Chem. Mater.*, 13 (2001) 3169-3183.
32. Y. S. Yun, S. Y. Cho, J. Shim, B. H. Kim, S. Chang, S. J. Baek, Y. S. Huh, Y. Tak, Y. W. Park, S. Park and H. Jin, *Adv. Mater.*, 25 (2013) 1993-1998.
33. M. Xiao, M. Huang, S. Zeng, D. M. Han, S. J. Wang, L. Sun and Y. Z. Meng, *RSC Adv.*, 3 (2013) 4914-4916.

34. M. N. Patel, X. Wang, D. A. Slanac, A. F. Domingo, D. Sheng, K. P. Johnston and K. J. Stevenson, *J. Mater. Chem.*, 22 (2012) 3160-3169.
35. W. Huang, H. Zhang, Y. Huang, W. Wang and S. Wei., *Carbon*, 49 (2011) 838–843.
36. E. Memarzadeh, P. Kalisvaart, A. Kohandehghan, D. Karpuzov and D. Mitlin., *J. Mater. Chem. A*, 2 (2014) 19685-19695.
37. Y. Korenblit, M. Rose, E. Kockrick, L. Borchardt, A. Kvit, S. Kaskel and G. Yushin, *ACS Nano*, 4 (2010) 1337-1344.
38. B. Ding, C. Yuan, L. Shen, G. Xu, P. Nie and X. Zhang, *Chem. Eur. J.*, 19 (2013)1013-1019.
39. G.M. Zhou, Y.B. Zhao and A. Manthiram, *Adv. Energy Mater.*, 5 (2015) 9.
40. Z. Li, L.X. Yuan, Z.Q. Yi, Y.M. Sun, Y. Liu, Y. Jiang, Y. Shen, Y. Xin, Z.L. Zhang and Y.H. Huang, *Adv. Energy Mater.* 1 (2014) 473.
41. W. Deng, X. Zhou, Q. Fang, and Z. Liu, *ChemNanoMat*, 2 (2016) 952-958.
42. K. Yang, Q. Ga, Y. Tan, W. Tian, W. Qian, L. Zhu and C. Yang, *Chem.Eur. J.*, 22 (2016) 3239-3244.
43. Y. Huang, M. Zheng, Z. Lin, B. Zhao, S. Zhang, J. Yang, C. Zhu, H. Zhang, D. Sun and Y. Shi, *J. Mater. Chem. A*, 3 (2015)10910.
44. Na, H., Lei, Z., Min, X., Wang, S., Han, D., Meng, Y. (2016). 3D Carbon Electrode for High-performance Battery Application. *Sci. Rep.*, 6 (2016) 33871.
45. X. Gu, Y. Wang, C. Lai, J. Qiu, S. Li, Y. Hou and W. Martens, *Nano Res.*, 8 (2015) 129-139.
46. M. Helen, M. A. Reddy, T. Diemant, U. Golla-Schindler, R. J. Behm, U. Kaiser, and M. Fichtner, *Sci. Rep.*, 5 (2015) 12146.
47. M. Yu, R. Li, Y. Tong, Y. Li, a C. Li, a J. Hong and G. Shi, *J. Mater. Chem. A*, 3 (2015) 9609-9615.
48. M. Park, J. Yu, K. J. Kim, G. Jeong, J. Kim, T. Yim, Y. Jo, U. Hwang, S. Kang, T. Woo, H. Kim and Y. Kim, *RSC Adv.*, 3 (2013) 11774-11781.
49. H. Wang, Z. Chen, H. K. Liu and Z. Guo, *RSC Adv.*, 4 (2014) 65074-65080.
50. J. Guo, J. Zhang, F. Jiang, S. Zhao, Q. Su, and G. Du, *Electrochim. Acta.*, 176 (2015) 853-860.
51. Z. Sun, S. Wang, L. Yan, M. Xiao, D. Han, Y. Meng, *J. Power Sources*, 324 (2016)547-555.
52. F. Wu, J. Li, Y. F. Su, J. Wang, W. Yang, N. Li, L. Chen and S. Chen, *Nano Letters*, 16 (2016)- 9.

© 2017 The Authors. Published by ESG ([www.electrochemsci.org](http://www.electrochemsci.org)). This article is an open access article distributed under the terms and conditions of the Creative Commons Attribution license (<http://creativecommons.org/licenses/by/4.0/>).